Simultaneous measurement of Young's and shear moduli of multiwalled carbon nanotubes using atomic force microscopy

Ganesh Guhados[a] and Wankei Wan
Department of Chemical and Biochemical Engineering, The University of Western Ontario, London, Ontario N6A 5B9, Canada

Xueliang Sun
Department of Mechanical and Materials Engineering, The University of Western Ontario, London, Ontario N6A 5B9, Canada

Jeffrey L. Hutter[b]
Department of Physics and Astronomy, The University of Western Ontario, London, Ontario N6A 3K7, Canada

(Received 30 July 2006; accepted 22 November 2006; published online 8 February 2007)

Carbon nanotubes (CNTs) are widely hailed as the strongest material known to mankind. However, experimental measurements—and even theoretical estimates—of their mechanical properties span a wide range. We present an atomic force microscopy study of multiwalled CNTs, which, unlike previous such studies, measures the tube compliance as a function of position along suspended tubes. This permits a simultaneous determination of the effective Young's and shear moduli of CNTs: 350±110 and 1.4±0.3 GPa, respectively. © *2007 American Institute of Physics*.
[DOI: 10.1063/1.2433125]

I. INTRODUCTION

The discovery of carbon nanotubes (CNTs) in 1991 fascinated the nanomaterials research community and triggered investigations of their structural, physical, and chemical properties.[1] Their excellent mechanical and electrical properties are now being exploited in diverse applications including field-emission displays,[2] nanosensors,[3] nanotweezers,[4] atomic-scale probes,[5] and composite materials.[6] There are two basic types of CNTs: a graphene sheet rolled seamlessly is referred to as a single-walled nanotube (SWNT), while a concentric series of SWNTs is referred to as a multiwalled nanotube (MWNT). By analogy to flat graphene sheets, the innate strength of the C–C bond suggests a Young's modulus of 1 TPa—the strongest material known to mankind. Particular interest in the fabrication of CNT-based composite materials is largely due to this high tensile strength coupled with flexibility and, in the case of MWNTs, low friction between the layers. CNTs are principally produced by arc discharge,[7] laser ablation,[8] and chemical vapor deposition.[9] However, catalytic chemical vapor deposition (CCVD) shows the most promise for scalability to large-scale production of low-cost products of high purity. The growth mechanism of CNTs is expected to have a significant effect on their mechanical properties; however, its details remain a topic of debate. Prior to routine fabrication of composite materials, the mechanical properties of individual nanotubes must be understood. Here, we detail our studies of the mechanical properties, namely, elastic and shear moduli, of multiwalled nanotubes.

An early study of the mechanical properties of MWNTs used the transmission electron microscope (TEM) to measure the amplitude of thermal fluctuations of cantilevered tubes, allowing a Young's modulus of 1.8±0.9 TPa to be deduced.[10] Further, Wong *et al.* and Salvetat *et al.* used the atomic force microscope (AFM) to measure the average Young's moduli as 1.28±0.59 and 0.81±0.41 TPa, respectively.[11,12] Yu *et al.* measured the tensile properties of MWNTs to report Young's moduli ranging from 270 to 950 GPa.[13,14] A surprisingly low Young's modulus ranging from 12 to 100 GPa has also been reported.[15] However, these low values were attributed to the misalignment of graphitic planes with the tube axis. Raman spectroscopic studies by Lourie and Wagner reported a Young's modulus ranging from 1.7 to 2.4 TPa.[16]

The mechanical properties of MWNTs have also been determined by numerical studies. One such study using first principles and empirical potential methods predicts a Young's modulus of 1.06 TPa;[17] however, Yakobson *et al.*[18] reported a value of 5.5 TPa. Thus, a rather scattered range of Young's moduli (from 0.5 to 5.5 TPa) has been reported in both experimental and numerical studies.

The ability of the AFM to map mechanical properties at the nanometer scale makes it the natural instrument for studying nanostructures. Previous AFM studies have used a single-point approach to study the strength of polypyrrole nanotubes,[19] poly (L-lactic acid) fibers,[20] and SWNT ropes.[21] In these cases, a known force was applied at a single point on a suspended nanotube, and Young's modulus determined from the resulting deflection. This technique, while valid, has some shortcomings. In addition to an inherently limited accuracy, the values obtained are highly reliant on the positional accuracy of the AFM scanner, which is often suspect for "open-loop" configurations, in which actual position is not measured. Further, a single-point measurement provides

[a]Present address: Axcelon Biopolymers Corp., London, Ontario, Canada.
[b]Author to whom correspondence should be addressed; electronic mail: jhutter@uwo.ca

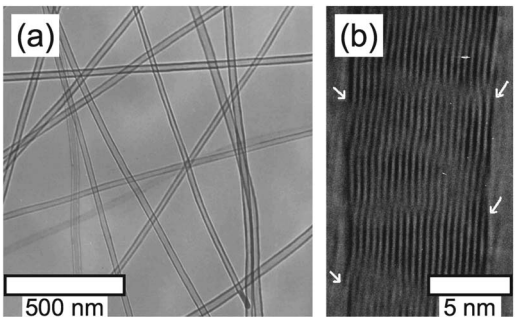

FIG. 1. (a) TEM micrograph of a MWNT. (b) HRTEM image of the wall showing layers with arrows indicating the scrolled structure.

no means of measuring the profile of the deflected tube and therefore of justifying the model employed, particularly if it relies on more than a single parameter. In some cases, this difficulty has been avoided by employing additional assumptions.[21,22] For instance, Salvetat *et al.* assumed a Young's modulus of $E=600$ GPa to determine a shear modulus in the range of 0.7–6.5 GPa for SWNTs of diameter of 4.5–20 nm.[21] Recently, we demonstrated the measurement of Young's modulus of bacterial cellulose nanofibers by measuring the fiber compliance at a series of positions.[23] Here, we extend this technique to characterize both elastic and shear properties of MWNTs, thus providing a direct experimental measurement of the shear modulus of MWNTs.

II. EXPERIMENT

Our MWNTs are produced by the chemical vapor deposition technique, in which a hydrocarbon gas is decomposed at elevated temperatures (~800 °C) on carbon fibers, on which Co/Ni particles are deposited as catalysts.[24] The size and chemistry of the catalyst play an important role in determining the diameter and wall thickness (i.e., number of concentric tubes) of the resulting structures. In our case, MWNTs with diameters ranging from 20 to 50 nm were produced. Figure 1(a) shows a TEM micrograph of a typical MWNT grown on carbon paper, while Fig. 1(b) shows the high-resolution TEM (HRTEM) image of the graphite layers.

The MWNTs thus produced were sonicated for 2 h in 70% (v/v) aqueous ethanol to obtain a suspension of tubes. A droplet of the suspension was placed on a polycarbonate membrane (Nucleopore track-etch membrane) of pore size of 0.8 μm and allowed to evaporate. The AFM experiments were performed using a MultiMode AFM with Nanoscope IIIa controller (Digital Instruments). Samples were imaged in air in contact mode using Si_3N_4 cantilevers with a nominal spring constant of 0.5 N/m. We used the thermal-noise technique[25] to determine an actual spring constant of 0.86 ± 0.03 N/m. Occasionally, tubes bridging a pore could be found, as shown in Fig. 2. Repeated imaging showed no tube displacement, indicating that the interaction between the polycarbonate surface and tubes was strong enough to clamp them to the membrane surface.

Nanomechanical testing was performed as previously reported[23] by acquiring "force-volume" images of 32×32 force spectra each, chosen to ensure that spectra (i.e., curves of AFM cantilever deflection y as a function of vertical

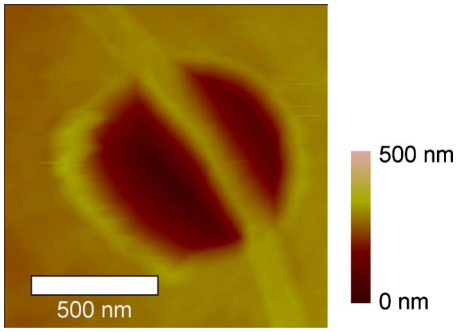

FIG. 2. (Color online) Atomic force microscope (AFM) image of a MWNT suspended across a pore in a polycarbonate membrane filter. The tube width is greatly exaggerated due to convolution with the pyramidal AFM tip.

sample displacement Δz) were collected at several positions on each tube. Vertical ramp sizes of 300 nm at a rate of 1 Hz were used, and the maximum force was limited to 56 nN to ensure that all measurements were within the elastic limit.

III. MECHANICAL MODEL

In the continuum limit, the elastic deflection of a clamped beam of length L due to bending caused by a force F applied at a point a measured from the edge of its suspended portion as illustrated in Fig. 3 is given by[26]

$$\delta_{\text{bend}}(x) = \begin{cases} (F/6EIL^3)[(L+2a)x-3La](L-a)^2x^2, & 0<x<a \\ (F/6EIL^3)[(L+2x)a-3Lx](L-x)^2a^2, & a<x<L, \end{cases} \tag{1}$$

where E is its Young's modulus (in the direction along the beam) and I is its area moment of inertia. For the case of a tubular beam, the area moment of inertia is given by $\pi(D^4-D_0^4)/64$, where D and D_0 are the outer and inner diameters, respectively, of the tube. At the particular location a at which the force is applied, the beam deflection is given by

$$\delta_{\text{bend}}(a) = \frac{F}{3EI}\left[\frac{a(L-a)}{L}\right]^3. \tag{2}$$

Because the deflection δ is linear in the applied force, the contact regimes of force spectra acquired at positions on the suspended tube reveal a uniform slope, which varies with position along the tube. We calibrate these slopes by normalizing to the mean value measured on the rigid substrate, where piezodisplacement is equal to cantilever deflection,

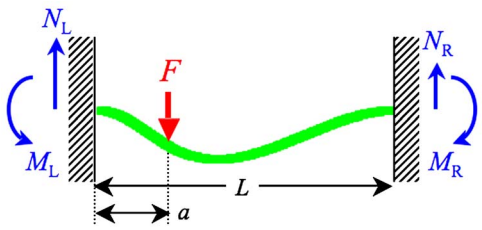

FIG. 3. (Color online) Schematic of a clamped beam of length L deflected by a force F applied at a point $x=a$. Indicated are the reaction forces N_L and N_R and moments M_L and M_R required to maintain the clamped boundary conditions at the left (L) and right (R) ends.

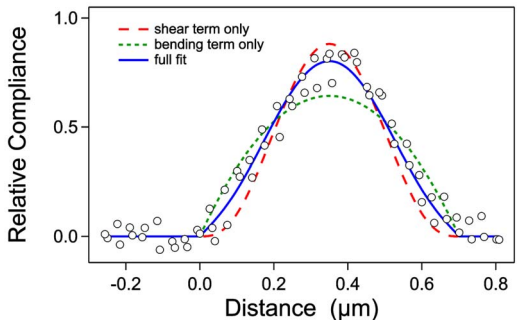

FIG. 4. (Color online) Compliance of suspended MWNTs as a function of position along the suspended portion of the tube measured relative to the cantilever compliance $1/k$. Fits to three models are indicated: one based on a simple bending model (dashed curve), one based solely on shear deformation (dotted curve), and one incorporating both deformation mechanisms described in Eq. (6) (solid curve). In general, both types of deformation must be considered to adequately model the data.

resulting in theoretical slopes of $dy/dz=1$. In order to extract the elastic parameters, we model the tube compliance—i.e., the ratio δ/F of its deflection to the applied force—as a function of position. Since the applied force is proportional to the cantilever deflection y, and the piezodisplacement Δz must be equal to $y+\delta$ once contact is achieved, we calculate the compliance at any position on the beam from the slope of the force spectrum acquired at that point according to

$$\frac{d\delta}{dF} \equiv \frac{1}{k}\frac{d\delta}{dy} = \frac{1}{k}\left[\left(\frac{dy}{dz}\right)^{-1} - 1\right]. \tag{3}$$

From Eq. (2), we can model the compliance as

$$\frac{d\delta}{dF} = \frac{64}{3\pi(D^4 - D_0^4)}\left[\frac{a(L-a)}{L}\right]^3 e, \tag{4}$$

where the parameter $e=1/E$. The outer diameters of the nanotubes and the length L of their suspended portions are determined from AFM height images. Following common practice,[21,22] the inner diameters, which cannot be measured by atomic force microscopy, are neglected. Figure 4 shows fits of the measured compliance determined according to Eq. (3) to the model of Eq. (4) (assuming $D_0=0$) for a typical data set.

It is clear from Fig. 4 that the pure-bending model does not capture the true behavior of the beam deflection. A better fit can be obtained by including an additional term: deflection due to shear. It is evident from Fig. 3 that any section of the suspended portion of the beam must be subject to a shear stress: for instance, for a section from the left support at $x=0$ to a point $x<a$ to be in mechanical equilibrium, an internal downward force at its right end must balance the supporting force N_L. We thus expect shear to result in an additional deflection of approximately $N_L x/GA$, where G is the shear modulus of the tube (measured radially) and $A=\pi(D^2-D_0^2)/4$ is its cross-sectional area. In fact, a more accurate calculation[26] shows that this deflection should be multiplied by a numerical factor f_s of order unity (for example, f_s ranges from 10/9 to 7/6 for a cylindrical beam, depending on its Poisson's ratio). We therefore approximate the shear deformation as that of a simply supported beam,[26]

$$\delta_{\text{shear}}(x) = \begin{cases} f_s(F/GAL)(L-a)x, & 0 < x < a \\ f_s(F/GAL)(L-x)a, & a < x < L, \end{cases} \tag{5}$$

so that the shear deformation at $x=a$ is $\delta_{\text{shear}}=f_s(L-a)aF/GAL$, and Eq. (4) becomes

$$\frac{d\delta}{dF} = \frac{64}{3\pi(D^4 - D_0^4)}\left[\frac{a(L-a)}{L}\right]^3 e + \frac{4f_s}{\pi(D^2 - D_0^2)}\frac{a(L-a)}{L}g, \tag{6}$$

where $g=1/G$.

In addition to the fit to the bending model of Eq. (1), Fig. 4 shows fits of a typical data set to a model considering shear alone, as well as to the full model of Eq. (6). Again, of necessity, we neglect the inner diameter D_0. It is clear that only the full fit is satisfactory; in particular, the shear term, which can typically be neglected for isotropic materials, cannot be excluded. By averaging the results of full fits to Eq. (6) of 13 data sets, we found Young's modulus of MWNTs to be 350 ± 110 GPa and their shear modulus to be 1.4 ± 0.3 GPa. It must be emphasized that because the model considers the MWNTs to be solid cylinders rather than hollow tubes, these moduli are underestimates—in reality, the intrinsic values for a graphene layer are higher. Nevertheless, we expect elastic properties measured in this way to be useful because they represent the effective moduli appropriate for predicting the mechanical behavior of these tubes. Moreover, even if the geometry were measured more accurately—e.g., by high-resolution TEM—the validity of extending continuum mechanics to an intrinsically atomic system has not been adequately tested.

IV. VALIDATION OF THE MECHANICAL MODEL

The mechanical measurements described above involve a number of assumptions. For instance, we assume that the tubes are well anchored to the substrate so that the clamped model is applicable. Because the AFM only records the portion of the sample in contact with the tip, we cannot directly show that all portions of the supported tube remain in contact with the substrate. However, we do note that the tubes remain in place through repeated scanning.

Implicit in the proposed bending model is an assumption that the lengths of the tubes do not change during the measurement. In reality, deflection must result in an increase in length. However, we find that this effect is not significant for the maximum deflections attained in this study. Within the context of the predicted beam profile [i.e., the sum of the deflections given by Eqs. (1) and (5)], the maximum tensile (and compressive) strains occur at the point of maximum curvature and have magnitude $D/2R$, where $R=[\delta''(x)]^{-1}$is the radius of curvature of the beam. It can be shown from Eq. (1) that the maximum tensile and compressive strains for a given applied force occur at the anchoring points when the force is applied a distance $a=L/3$ away and are given by $\varepsilon_{\max}=2DLF/27EI$. In the case of our measurements, we estimate that the maximum strains due to bending range from 0.1% to 1%. In contrast, the maximum strains due to the increase in the contour length of the tubes, which we over-

estimate as $2\delta_{max}/L = FL^2/96EI + f_s FL/4GA$, where δ_{max} is the predicted maximum deflection, were typically an order of magnitude smaller. It should be noted that for forces higher than those used in our analysis we do see the expected transition to nonlinear force curves. We did not attempt to extend our analysis to such cases and restricted the force range employed where necessary.

The maximum strain allows us to calculate the maximum load sustained by any portion of the MWNTs during measurement. The fact that the tubes were able to sustain strains as high as 1% implies that the tensile strength of the tubes is at least several gigapascals (actual loads varied from 1 to 12 GPa). Again, this is an effective value assuming a load distributed across the entire tube cross section—the intrinsic value for the tube walls must be higher. This lower bound on the tensile strength is consistent with previous measurements of MWNTs.[13]

V. DISCUSSION

Most experimentally determined values of Young's modulus of MWNTs fall over a wide range of 0.4–2.4 TPa, though a much higher value of about 3.7 TPa has also been reported for tubes of smaller diameters.[10,27] Some of this variation may be due to differences in the method of production. Salvetat *et al.* noted a large difference in Young's modulus of arc-discharge MWCNTs, 1.28±0.59 TPa, relative to those produced by CCVD using NaY zeolite as catalyst, for which values as low as 50 GPa were reported.[27]

Although our estimate of 350 GPa for Young's modulus of MWNTs is within the range of previous experimental reports, the large standard error of 110 GPa in our mean value indicates that there is more to the story. One possible explanation for the scatter in our values is that the similarity in shape between the bending and shear terms in Eq. (5) results in a strong covariance between the fit parameters e and g, making independent determination of Young's and shear moduli difficult. Another possibility is the variation in the defect density, which has been recently studied by Gaillard *et al.*[30]

Intrinsic variations between the tubes will likely play an important role, even for defect-free samples. Iijima[31] demonstrated that for tubes of comparable diameters, the number of inner layers, and therefore the wall thickness, can differ. However, the inner diameter cannot be measured in an AFM experiment. This variability significantly affects the effective value of the modulus. Thus, models that assume a cylindrical geometry (as do Refs. 12, 15, 21, 22, and 27 as well as ourselves) underestimate the intrinsic material properties.

The shear moduli of MWNTs have been estimated by theoretical simulations to be 0.45 TPa (Ref. 28) and 0.4±0.05 TPa (Ref. 29). The value of 1.4±0.3 GPa we measure is similar to the 1 GPa range estimated by Salvetat *et al.* for ropes of multiple SWNTs, in which individual tubes may slide past each other, but is much lower than the expected value for single tubes.[21] Experimental studies have established the ability to separate and pull out individual layers of MWNTs under tensile load.[13] Forces applied along a nanotube might therefore result in interlayer slipping, leading to a low shear modulus since layers, such as adjacent graphene sheets in graphite, are bound only by weak van der Waals interactions.

The surprisingly low value of the shear modulus may provide important clues about the structure of MWNTs. It is known that MWNTs not only form concentric layers of graphene sheets but can also form scroll-like structures, in which one or more graphene sheets are wrapped up to form nanotubes with inner layers similar to those of MWNTs.[32,33] These scrolled and nested structures of MWNTs have been widely discussed, but are often referred to as defects in the regular MWNT growth process. For instance, Lavin *et al.*[34] reported HRTEM observations suggesting the coexistence of scrolled and nested features. A growth model proposed by Amelinckx *et al.*[35] predicts that nested and scroll-type structures would be present side by side. Recently, Sun *et al.*[36] have demonstrated the scrolled structure of our MWNT samples by direct observations by HRTEM. In this case, the cylindrical tube is generated by a single graphene sheet. As seen in Fig. 1(b), the graphene layers present a small angle with the tube's axis, also confirming a scrolled structure. We believe that the increased potential for interlayer slipping in a scrolled structure contributes to the observed low shear modulus.

VI. THE REDUCED MODULUS

In order to explore the cause of scatter in our results, we characterize the tube compliance by a single parameter, the "reduced modulus" at the tube center defined by Salvetat *et al.*[21] as

$$E_r = \frac{L^3}{3\pi D^4} \frac{1}{d\delta/(dF)|_{a=L/2}} \tag{7}$$

(after correcting a typographical error in Ref. 21). This empirical quantity reduces to Young's modulus in the case of a solid cylinder with negligible shear deformation, but is smaller in general. We use the results of fits to Eq. (6) as smoothing functions to determine the value of compliance at the tube center far more accurately than could be achieved by a single-point measurement and to provide, through the covariance matrix, an estimate of the uncertainty in the reduced modulus.

Figure 5 plots the reduced modulus E_r as a function of tube diameter (the suspended length is approximately the same in all cases). This quantity apparently decreases with increasing diameter, though more data points at smaller diameters (~15 nm) would be necessary to establish a trend. In order to understand this trend, we use Eq. (6) to show the expected behavior as a function of the wall thickness expressed as the number of layers (assuming an interlayer spacing of 0.34 nm). Several sample curves are shown, but the scatter in the data, which is presumably due to both defects and variations in the number of layers, makes definitive conclusions impossible. We note, however, that no reasonable model of this sort can simultaneously match the values of the effective modulus over the entire range of diameters studied unless Young's modulus is less than 1 TPa and the shear modulus is not more than a few gigapascals. The family of

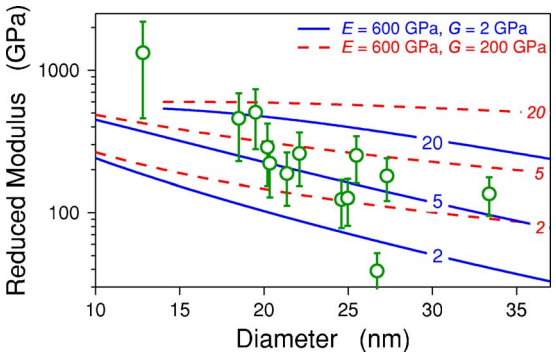

FIG. 5. (Color online) Reduced modulus of MWNTs as a function of tube diameter. Two families of models are shown for comparison. The solid curves show the expected behavior for tubes with a Young's modulus of 600 GPa, but a low shear modulus of 2 GPa, and a varying number of layers (indicated by the column of numbers near diameter of 30 nm). The dashed curves indicate expectations for tubes with a shear modulus that is a sizable fraction of Young's modulus, which is chosen as 200 GPa for the purposes of this illustration (the number of layers is indicated by the numbers on the right-hand side). Although both models encompass most of the data, the trend of a reduced modulus that decreases with tube diameter favors the first model.

solid curves shows the expected behavior for a Young's modulus of 600 GPa and a shear modulus of 2 GPa, with a varying number of layers. This set of curves is able to encompass most of the data: significantly lower choices of E are unable to match the experimental values of E_r at small diameters, whereas higher values suggest that the tubes must contain fewer layers than typically observed by TEM for samples from the batch studied. We note that such a low value of the intrinsic shear modulus of the tubes is consistent with the *effective* value of 1.4 GPa determined earlier (by treating the tubes of unknown inner diameter as cylinders); indeed, the fact that the tube compliance could not be modeled as a pure bend strongly suggests a small shear modulus. An alternative family with a shear modulus of 200 GPa (dashed curves) does a much poorer job: while it does span the measured values of the reduced modulus, it would require tubes of smaller diameter to systematically have thicker walls.

VII. CONCLUSIONS

We have developed a technique to directly determine effective values of both Young's and shear moduli of MWNTs. We measured a Young's modulus of 350 ± 110 GPa, which is consistent with previous experimental estimates and lower than theoretical predictions. We reported a direct measurement of the shear modulus ($G = 1.4 \pm 0.3$ GPa) of MWNTs, which is much lower than theoretical estimates. Because the inner diameter of the tubes could not be measured in our experiment, these values describe the elastic properties of the entire tube, not the intrinsic properties of the graphene layers of which it is comprised. A consideration of the variation of the elastic properties with tube diameter suggests that the intrinsic Young's modulus of the tube wall alone is smaller than 1 TPa, while the intrinsic shear modulus must be of the order of only a few gigapascals. Given the sensitivity of these results to assumptions about the inner structure of the nanotubes, as highlighted by Fig. 5, we suggest that high-resolution imaging of specific tubes, perhaps by TEM, is essential for future experimental efforts and will also permit numerical modeling to proceed beyond the classical beam theory.

ACKNOWLEDGMENTS

We thank the Canada Foundation For Innovation (CFI) for funding of the atomic force microscope infrastructure and NSERC (Canada) for operational support. One of us (G.G.) thanks the University of Western Ontario for an International Graduate Student Scholarship.

[1] S. Iijima, Nature (London) **354**, 56 (1991).
[2] Y. T. Feng, S. Z. Deng, J. Chen, and N. S. Xu, Ultramicroscopy **95**, 93 (2003).
[3] S. Hrapovic, Y. Liu, K. B. Male, and J. H. T. Luong, Anal. Chem. **76**, 1083 (2004).
[4] P. Kim and C. M. Lieber, Science **286**, 2148 (1999).
[5] C. V. Nguyen, Q. Ye, and M. Meyyappan, Meas. Sci. Technol. **16**, 2138 (2005).
[6] D. Pantarotto, J.-P. Briand, M. Prato, and A. Bianco, Chem. Commun. (Cambridge) **2004**, 16.
[7] T. W. Ebbesen and P. M. Ajayan, Nature (London) **358**, 220 (1992).
[8] J.-F. Colomer, L. Henrard, Ph. Lambin, and G. van Tendeloo, Eur. Phys. J. B **27**, 111 (2002).
[9] E. Flahaut, R. Bacsa, A. Peigney, and C. Laurent, Chem. Commun. (Cambridge) **2003**, 1442.
[10] M. M. J. Treacy, T. W. Ebbesen, and J. M. Gibson, Nature (London) **381**, 678 (1996).
[11] E. W. Wong, P. E. Sheehan, and C. M. Lieber, Science **277**, 1971 (1997).
[12] J. P. Salvetat, J. M. Bonard, N. H. Thomson, A. J. Kulik, L. Forro, W. Benoit, and L. Zuppiroli, Appl. Phys. A: Mater. Sci. Process. **69**, 255 (1999).
[13] M.-F. Yu, O. Lourie, M. J. Dyer, K. Moloni, T. F. Kelly, and R. S. Ruoff, Science **287**, 637 (2000).
[14] M.-F. Yu, B. S. Files, S. Arepalli, and R. S. Ruoff, Phys. Rev. Lett. **84**, 5552 (2000).
[15] B. Lukic *et al.*, Appl. Phys. A: Mater. Sci. Process. **80**, 695 (2005).
[16] O. Lourie and H. D. Wagner, J. Mater. Res. **13**, 2418 (1998).
[17] D. H. Robertson, D. W. Brenner, and J. W. Mintmire, Phys. Rev. B **45**, 12592 (1992).
[18] B. I. Yakobson, C. J. Brabec, and J. Bernholc, Phys. Rev. Lett. **76**, 2511 (1996).
[19] S. Cuenot, S. Demoustier-Champagne, and B. Nysten, Phys. Rev. Lett. **85**, 1690 (2000).
[20] E. P. S. Tan and C. T. Lim, Appl. Phys. Lett. **84**, 1603 (2004).
[21] J.-P. Salvetat, G. A. D. Briggs, J.-M. Bonard, R. R. Bacsa, A. J. Kulik, T. Stockli, N. A. Burnham, and L. Forro, Phys. Rev. Lett. **82**, 944 (1999).
[22] B. Lukic *et al.*, Nano Lett. **5**, 2074 (2005).
[23] G. Guhados, W. Wan, and J. L. Hutter, Langmuir **21**, 6642 (2005).
[24] X. Sun, R. Li, B. Stansfield, J. P. Dodelet, and S. Desilets, Chem. Phys. Lett. **394**, 266 (2004).
[25] J. L. Hutter and J. Bechhoefer, Rev. Sci. Instrum. **64**, 1868 (1993).
[26] S. Timoshenko and J. M. Gere, *Mechanics of Materials*, 4th ed. (PWS, Boston, MA, 1997).
[27] J.-P. Salvetat *et al.*, Adv. Mater. (Weinheim, Ger.) **11**, 161 (1999).
[28] J. P. Lu, Phys. Rev. Lett. **79**, 1297 (1997).
[29] C. Li and T.-W. Chou, Compos. Sci. Technol. **63**, 1517 (2003).
[30] J. Gaillard, M. Skove, and A. M. Rao, Appl. Phys. Lett. **86**, 233109 (2005).
[31] S. Iijima, Mater. Sci. Eng., B **19**, 172 (1993).
[32] W. Ruland, A. K. Schaper, H. Hou, and A. Greiner, Carbon **41**, 423 (2003).
[33] S. F. Braga, V. R. Coluci, S. B. Legoas, R. Giro, D. S. Galvao, and R. H. Baughman, Nano Lett. **4**, 881 (2004).
[34] J. G. Lavin, S. Subramoney, R. S. Ruoff, S. Berber, and D. Tomanek, Carbon **40**, 1123 (2002).
[35] S. Amelinckx, D. Bernaerts, X. B. Zhang, G. Van Tendeloo, and J. Van Landuyt, Science **267**, 1334 (1995).
[36] X. Sun, R. Li, B. Stansfield, J.-P. Dodelet, G. Ménard, and S. Désilets, Carbon (in press).